

Some Improvements in Elastoplastic Friction Compensator¹

Masayoshi IWATANI* and Ryo KIKUWE*

Abstract : For robotic joints with compliant transmissions, Mahvash and Okamura have proposed a friction compensator based on an elastoplastic friction model. One drawback of the compensator is that the compensator continues producing non-zero output force in the static friction state, which results in the degraded backdrivability of joints. In order to remedy this problem, this paper proposes an elastoplastic friction compensator with improved static friction behavior, which is realized by an additional term that makes the output force exponentially decay in the static friction state. This paper also proposes an additional algorithm that adjust the decay rate of the output force in real time. The proposed methods are experimentally tested with a linear actuator with a timing belt and a six-axis industrial manipulator.

Key Words : friction compensation, static friction, dither.

1. Introduction

In robotic systems, joint friction is one of major factors that degrade the backdrivability of the joint and the accuracy of control. One straightforward idea to handle this problem is friction compensation, i.e., generating actuator force canceling the friction force. To find an appropriate compensator, however, is not a trivial problem. One major factor of the difficulty is that the friction force is generally formulated as a discontinuous function of the sliding velocity. Inappropriate treatment of the discontinuities leads to high frequency oscillation in the actuator force in the neighborhood of the zero velocity.

One of the simplest friction models is Hayward and Armstrong's [2] friction model. Their friction model can be seen as an elastoplastic friction model, which is composed of a serial connection of an elastic component and a Coulomb-friction component. Some other friction models can be seen as extensions of Hayward and Armstrong's model. For example, Dupont et al.'s model [3] is an elastoplastic friction model with a sophisticated presliding behavior. Kikuuwe et al. [4] have proposed a viscoelasto-plastic model, which includes non-zero viscosity in the presliding region. Xiong et al.'s model [5] is a multi-state friction model, which is composed of multiple viscoelasto-plastic elements connected in parallel.

The originally intended application of Hayward and Armstrong's elastoplastic friction model [2] is haptic rendering, in which artificial friction forces are generated by the actuators. Mahvash and Okamura [6], however, employed their model for the purpose of friction compensation, in which the real friction forces are canceled by the actuator forces. They applied their technique for a tendon-driven mechanism, in which the compliance of the tendon corresponds to the compliance of the elastoplastic friction model. A similar idea has also been employed by the authors [7], in which a multi-state viscoelasto-

plastic friction model was used for friction compensation of a harmonic drive transmission. Tjahjowidodo et al. [8] also developed a friction compensator for a harmonic drive based on a multi-state friction model [9].

In this paper, we focus on a flaw of the elastoplastic friction compensators, which has not been pointed out in previous studies. The flaw is that, in the static friction state, the compensator continues generating non-zero actuator force caused by the imaginary elastic displacement in the compensator. This unnecessary output force hampers the sensitivity of the joint against the external force. Motivated by this observation, this paper proposes an improved elastoplastic friction compensator, which includes an additional term that makes the output force exponentially decay in the static friction state. We also combine this new method with a sinusoidal dither-like actuation in the static friction state to further enhance the sensitivity of the system against external forces. Moreover, we propose an additional algorithm for the compensator, with which the decay rate of the output force is adjusted in real time to realize a better behavior of the system both kinetic and static friction states.

The content of the paper has been partially presented in our prior conference publication [1]. Newly added contribution of the present paper is the new additional algorithm that adjusts the decay rate and new experimental results obtained with an industrial manipulator with harmonic-drive transmissions.

The rest of this paper is organized as follows. Section 2 shows our experimental setups. Section 3 overviews Mahvash and Okamura's elastoplastic friction compensator. Section 4 presents a new elastoplastic friction compensator, which alleviates the flaw of Mahvash and Okamura's method. Section 5 shows experimental results of the proposed compensator. Section 6 presents the additional algorithm for the online adjustment of the decay rate, and also shows some experimental results. Section 7 provides some concluding remarks.

2. Experimental Setups

2.1 Overview

Experiments in this paper employ two experimental devices, which are shown in Fig. 1. Setup A, shown in Fig. 1 (a), consists of an AC servomotor, in which an optical encoder is embedded,

* Department of Mechanical Engineering, Kyushu University, 744 Motoooka, Nishi-ku, Fukuoka, 819-0395, Japan
E-mail: iwatani@ctrl.mech.kyushu-u.ac.jp, kikuuwe@mech.kyushu-u.ac.jp

(Received October 25, 2016)

(Revised December 17, 2016)

¹ This paper extends the authors' previous conference paper [1].

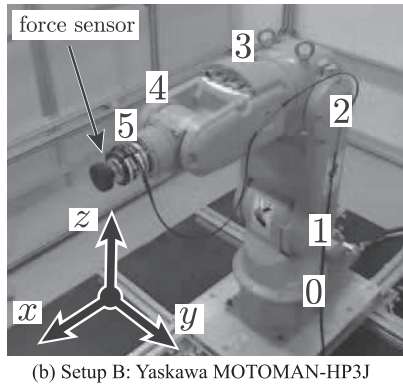
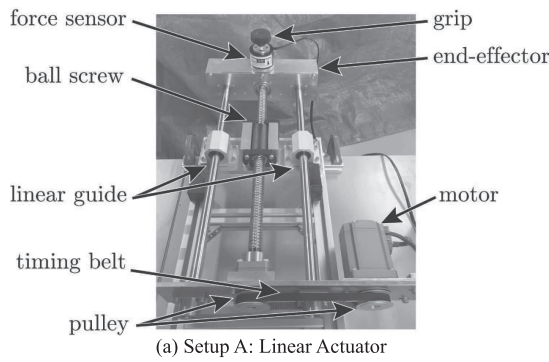


Fig. 1 Experimental setups.

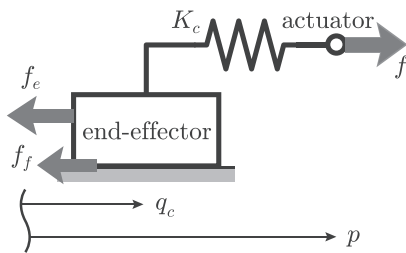


Fig. 2 Schematic illustration of the setups.

and a ball screw connected through a timing belt and pulleys to the servomotor. In this device, the end-effector and the actuator are connected through a compliant transmission, i.e., the timing belt. Setup B, shown in Fig. 1 (b), is a six-axis industrial manipulator MOTOMAN-HP3J, Yaskawa Electric Corporation. Each joint of the setup has an AC servomotor, an optical encoder and a harmonic drive transmission, which has compliance.

In each of the setups, the friction mostly exists on the end-effector's side, not on the actuator and the optical encoder's side. This feature raises a difficulty in the friction compensation because the end-effector's velocity cannot be measured directly with the optical encoder.

The mechanism structures of the setups can be schematically illustrated as in Fig. 2. Here, p and q_c represent the position of the actuator and the end-effector, respectively, K_c is the elasticity of the compliant transmission, f_f is the friction force on the side of the end-effector, f is the force of the actuator, and f_e is external forces acting on the end-effector. This arrangement of the friction and the compliance is the same as that of Mahvash and Okamura [6], where a tendon-driven joint is modeled in the same way as Fig. 2.

As for Setup A, the linear actuator, the rated power of the

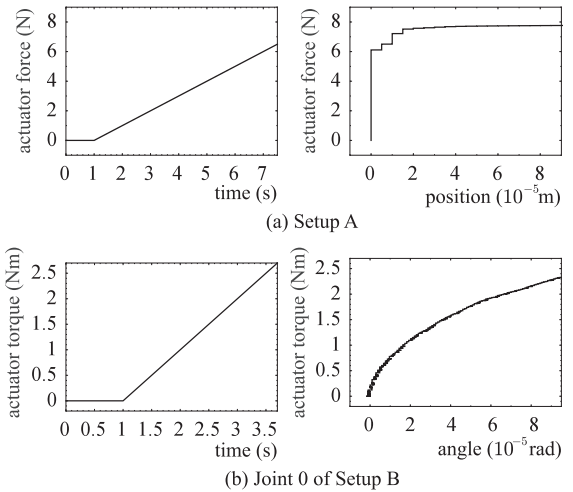


Fig. 3 Presliding properties of the setups.

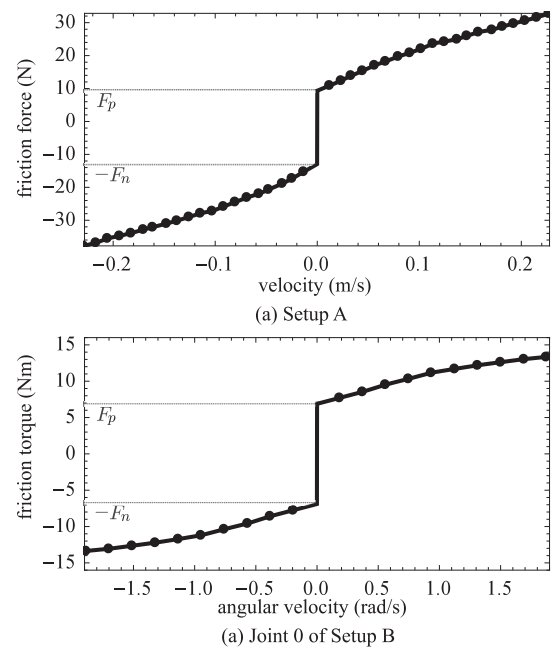


Fig. 4 Identification result of rate-dependent friction.

actuator is 200 W, the lead of the ball screw is 0.02 m, and the resolution of the encoder is 4000 counts per rotation. As for Setup B, the industrial manipulator, we used only the three joints from the base. In these three joints (Joints 0, 1 and 2), all the actuators' rated power is 80 W, and all the encoders' resolution is 65,536 counts per rotation, and the reduction ratios of the transmissions are 100, 224 and 120, respectively. During the experiments, a force sensor NITTA IFS-50M31A25-I25 was attached to the end-effector of each setup to measure the external forces.

2.2 Presliding Behaviors

Preliminary experiments were performed to clarify the presliding behaviors of our setups. In these experiments, ramp-type force input was applied to the joints by the actuators. Figure 3 shows the result. Figure 3 (a) shows that the measured displacement of Setup A is zero as long as the actuator force is smaller than 6 N. On the other hand, in Fig. 3 (b), Joint 0 of MOTOMAN-HP3J exhibits significant presliding displacement under small actuator torque.

The difference of the presliding behaviors between the two setups can be attributed to the differences in the stiffness of the transmission and the resolution of the encoders. In the case of Setup A, due to the high stiffness of the timing belt, the elongation of the belt was smaller than displacement for one count of the encoder step. On the other hand in the case of Setup B, the resolution of the encoder is high enough to observe small displacement under small torque.

2.3 Identification of Rate-Dependent Friction

In order to investigate the relation between the velocity and the friction force in our setups, we used our previously proposed procedure [10], which is for the identification of rate-dependent friction law. The procedure was slightly modified to deal with different magnitudes of friction in different directions. Figure 4 shows the obtained data and curves from the procedure. Here we describes the curves in the following form:

$$f \in \text{gsign}(-F_n, v, F_p) + \Phi(v) \quad (1)$$

where F_p and F_n are positive constants, $\Phi(\cdot)$ is a continuous function that satisfies $\Phi(0) = 0$, and gsign is the generalized signum function defined as follows:

$$\text{gsign}(A, x, B) \triangleq \begin{cases} B & \text{if } x > 0 \\ [A, B] & \text{if } x = 0 \\ A & \text{if } x < 0. \end{cases} \quad (2)$$

The function $\Phi(\cdot)$ and the constants F_p and F_n are obtained by the linear interpolation and extrapolation of the sampled velocity-friction force pairs. Figure 4 (a) shows that, in Setup A, the magnitudes of friction are different in different directions, i.e., $F_p \neq F_n$, and the curve of the rate-dependent friction is almost straight. Figure 4 (b) shows that, in Setup B, the magnitude of friction is almost symmetric with respect to velocity $v = 0$. We use the identified F_p , F_n and $\Phi(\cdot)$ in the proposed compensator.

3. Previous Elastoplastic Friction Compensator

3.1 Friction Model on Which Previous Compensator Is Based

Hayward and Armstrong's elastoplastic friction model [2] is a serial connection of an elastic element and a Coulomb friction element. Their model is originally presented in the discrete-time domain. In their model, the algorithm to obtain the friction force f_k from the input position p_k , where k is the discrete-time index, can be written as follows:

$$q_k := p_k - \frac{F}{K} \text{sat}\left(\frac{K}{F}(p_k - q_{k-1})\right) \quad (3a)$$

$$f_k := K(p_k - q_k) \quad (3b)$$

where $\text{sat}(\cdot)$ is a unit saturation function defined as follows:

$$\text{sat}(x) \triangleq \begin{cases} x/|x| & \text{if } |x| > 1 \\ x & \text{if } |x| \leq 1. \end{cases} \quad (4)$$

Here, F represents the magnitude of the Coulomb friction force, K represents the spring coefficient of the elastic element, and q_k is a state variable representing the position of the Coulomb friction element.

Kikuuwe et al.'s [4] friction model is also presented in the discrete-time domain and can be seen as a generalization of the

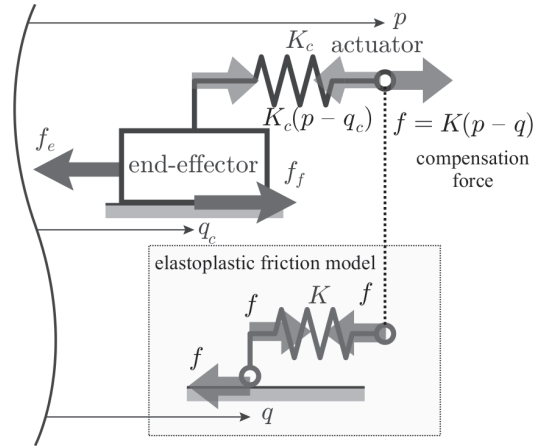


Fig. 5 Elastoplastic friction compensator applied to an elastic joint.

model (3) with a non-zero presliding viscosity. They have also presented the relation between continuous-time and discrete-time representations through the backward Euler discretization. In particular, based on Kikuuwe et al.'s way of derivations, the continuous-time counterpart of the algorithm (3) can be written as follows:

$$K(p - q) \in F \text{sgn}(\dot{q}) \quad (5a)$$

$$f = K(p - q) \quad (5b)$$

where $\text{sgn}(\cdot)$ is the set-valued signum function defined as follows:

$$\text{sgn}(x) \triangleq \begin{cases} x/|x| & \text{if } |x| \neq 0 \\ [-1, 1] & \text{if } |x| = 0. \end{cases} \quad (6)$$

The function $\text{sgn}(\cdot)$ possesses the following property:

$$\text{sgn}(kx) = \text{sgn}(x) \quad \forall k > 0 \quad (7)$$

and it is connected to $\text{sat}(\cdot)$ by the following relation:

$$y \in \text{sgn}(x - y) \iff y = \text{sat}(x), \quad (8)$$

of which the proof is presented in [11]. By substituting (5) by $\dot{q} := (q_k - q_{k-1})/T$ where T is the time-step size, one can obtain the algorithm (3) through the relation (8). The details of the derivation can be found in [4],[11]. The set of simultaneous differential equations (5), and its discrete-time counterpart (3), can be seen as the simplest form of an elastoplastic model, which is a serial connection of the elasticity and the Coulomb friction. In this model, as can be seen in (5a), the spring force, the left-hand side, always balances the Coulomb friction force, the right-hand side.

3.2 Problem of Previous Friction Compensator

For friction compensation of a tendon-driven joint, Mahvash and Okamura [6] have employed an algorithm that can be written as (3). A schematic illustration of this implantation is shown in Fig. 5. The compensation force f is computed based on the model, i.e., the algorithm (3), according to the input position p .

One problem that we noticed through some preliminary experiments is that, even when p and q do not coincide with each other, the system may be in an equilibrium due to the stiction both in the device and in the model. In this case, the compensator continues producing the non-zero output force f , while

the end-effector stays in the static friction state. This situation is not preferable because, to break away this static friction state, an external force f_e larger than the static friction level may be required. That is, in the static friction state, the output of the compensator degrades the device's sensitivity to external forces.

4. Proposed Friction Compensator

4.1 Main Contribution: Exponentially Decaying Output Force

Here we present a new friction compensator that avoids the problem explained in Section 3.2. The source of the problem is the dislocated equilibrium between p and q , which results in the continuing non-zero output force f in the static friction. In order to prevent this, we propose a modified version of (5) as follows:

$$K(p - q) \in F \operatorname{sgn}(\dot{q} + \alpha(q - p)) \quad (9a)$$

$$f = K(p - q) \quad (9b)$$

where α is a positive constant.

In the compensator (9), the additional term $+\alpha(q - p)$ has the effect of preventing the equilibrium at $q - p \neq 0$. Equation (9a) can be equivalently rewritten as follows:

$$\begin{aligned} & ((K(p - q) = F) \wedge (\dot{q} + \alpha(q - p) > 0)) \\ & \vee ((|K(p - q)| < F) \wedge (\dot{q} + \alpha(q - p) = 0)) \\ & \vee ((K(p - q) = -F) \wedge (\dot{q} + \alpha(q - p) < 0)), \end{aligned} \quad (10)$$

which can be further rewritten as follows:

$$\begin{aligned} & ((\dot{q} > \alpha F/K) \wedge (K(p - q) = F)) \\ & \vee ((\dot{q} = -\alpha(q - p)) \wedge (|K(p - q)| < F)) \\ & \vee ((\dot{q} < -\alpha F/K) \wedge (K(p - q) = -F)). \end{aligned} \quad (11)$$

This implies that, when $K(p - q) = f \in (-F, F)$, i.e., when the compensator is in the static friction state, q exponentially converges to p and the parameter α determines the rate of convergence. Meanwhile, when $K(p - q) = f$ is either $+F$ or $-F$, i.e., when the compensator is in the kinetic friction state, the velocity \dot{q} is larger than $\alpha F/K$. That is, the parameter α determines the threshold value $\alpha F/K$ above which the compensator produces a constant force. The former effect indeed prevents the dislocated equilibrium at $p \neq q$ although the latter effect is not what we exactly intended.

Here we derive the algorithm of the compensator based on the simultaneous differential equations (9). The backward Euler discretization of (9a) can be written as follows:

$$K(p_k - q_k) \in F \operatorname{sgn}\left(\frac{q_k - q_{k-1}}{T} + \alpha(q_k - p_k)\right), \quad (12)$$

which is equivalent to

$$\frac{K}{F}(p_k - q_k) \in \operatorname{sgn}\left(\frac{K(p_k - q_{k-1})}{F(1 + T\alpha)} - \frac{K}{F}(p_k - q_k)\right). \quad (13)$$

By the application of the relation (8), one can see that (13) is equivalent to the following:

$$\frac{K}{F}(p_k - q_k) = \operatorname{sat}\left(\frac{K(p_k - q_{k-1})}{F(1 + T\alpha)}\right), \quad (14)$$

which is equivalent to

$$q_k = p_k - \frac{F}{K} \operatorname{sat}\left(\frac{K(p_k - q_{k-1})}{F(1 + T\alpha)}\right). \quad (15)$$

Consequently, the discrete-time algorithm of the proposed friction compensator is written as follows:

$$q_k := p_k - \frac{F}{K} \operatorname{sat}\left(\frac{K(p_k - q_{k-1})}{F(1 + T\alpha)}\right) \quad (16a)$$

$$f_k := K(p_k - q_k). \quad (16b)$$

The compensator (16) is built on the assumption that the device friction is the pure Coulomb friction, i.e., $f = F \operatorname{sgn}(v)$. If the friction force is rate-dependent as in (1) and Fig. 4, the continuous-time representation of the compensator (9) should be slightly generalized as follows:

$$K(p - q) \in \operatorname{gsgn}(-F_n, \dot{q} + \alpha(q - p), F_p) \quad (17a)$$

$$f = K(p - q) + \Phi(\dot{q}). \quad (17b)$$

A straightforward derivation shows that, through the backward Euler discretization, a discrete-time algorithm correspondent to (17) can be obtained as follows:

$$q_k := p_k - \frac{1}{K} \operatorname{gsat}\left(-F_n, \frac{K(p_k - q_{k-1})}{1 + T\alpha}, F_p\right) \quad (18a)$$

$$f := K(p_k - q_k) + \Phi\left(\frac{q_k - q_{k-1}}{T}\right). \quad (18b)$$

Here, gsat is a generalized saturation function defined as follows:

$$\operatorname{gsat}(A, x, B) \triangleq \begin{cases} B & \text{if } x > B \\ x & \text{if } x \in [A, B] \\ A & \text{if } x < A, \end{cases} \quad (19)$$

and the following properties of gsgn and gsat are used in the derivation:

$$\operatorname{gsgn}(A, \kappa x, B) = \operatorname{gsgn}(A, x, B) \quad \forall \kappa > 0 \quad (20)$$

$$y \in \operatorname{gsgn}(A, x - y, B) \iff y = \operatorname{gsat}(A, x, B). \quad (21)$$

The functions gsgn and gsat have been introduced in [11] where a proof for the relation (21) is also included.

The performance of the algorithm (18) cannot be very sensitive to the choice of the time-step size T because both functions gsat and Φ are continuous and thus the algorithm does not involve any discontinuities. The parameter α should be chosen according to the required convergence rate of the compensation force. Note that α is not a model parameter of the controlled object, but a design parameter that should be chosen according to the purposes of applications.

4.2 Algorithm

The output force f of the algorithm (16), or its generalized version (18), exponentially decays to zero during the static friction state. Therefore, it does not facilitate the breaking away from the static friction state according to external forces below the maximum static friction level. Thus, we combine the algorithm (18) with a dither-like actuation that is activated only in the static friction state. The purpose here is to improve the system's sensitivity to external forces by maintaining the system on the verge of the static friction state. We choose a simple sinusoidal signal for the dither actuation, and its amplitude is chosen so that it causes oscillation of a few encoder counts.

The frequency of the signal is chosen so that it is higher than the supposed frequency component of the external force. In our case, because we are considering the application in which the robot is manually moved by human hand, it is set higher than the frequency of typical human voluntary movement. such as 5 Hz.

In conclusion, we here propose the following algorithm as a friction compensator:

Function **algFC**(p_k, α) (22a)

$$f_m^* := \frac{K(p_k - q_{k-1})}{1 + T\alpha} \quad (22b)$$

$$q_k := p_k - \frac{1}{K} \text{gsat}(-F_n, f_m^*, F_p) \quad (22c)$$

$$f_m := K(p_k - q_k) \quad (22d)$$

$$\text{If } -F_n < f_m^* < F_p \quad (22e)$$

$$f_d := R_d \left(\frac{F_p + F_n}{2} \sin(\Omega_d t) + \frac{F_p - F_n}{2} \right) \quad (22f)$$

Else (22g)

$$f_d := 0 \quad (22h)$$

Endif (22i)

$$f := f_m + f_d + \Phi((q_k - q_{k-1})/T) \quad (22j)$$

Return f . (22k)

Here, the newly introduced parameters R_d and Ω_d , which determines the amplitude and the frequency of the dither signal, are chosen according to the aforementioned guideline.

A similar idea to use the dither-like signal has been presented by Aung et al. [12]. They used a more sophisticated method, in which the dither signal is a saw wave-like signal and the signal reversal is triggered by the change in the encoder counts. The combination of our main contribution, (18), and such a sophisticated dither technique is left for future study.

5. Experiments

The proposed method was tested with Setup A and Setup B, which are shown in Fig. 1. In this experiments, the following five cases were compared:

- **NC**: no compensation.
- **C**: the compensator **algFC** in (22) with $\alpha = 0$ without dither (i.e., $R_d = 0$). It is a trivial extension of the conventional Mahvash and Okamura's compensator.
- **CD**: **C** with dither.
- **P**: the compensator **algFC** in (22) with $R_d = 0$, i.e., the proposed method without dither.
- **PD**: the proposed compensator **algFC** in (22).

Throughout all experiments in this paper, the time-step size (the sampling interval) was set as $T = 0.001$ s.

5.1 Experiment: Setup A

Here we show experimental results with Setup A. The experimenter grasped the grip attached to the force sensor and moved the end-effector by hand. The experimenter intended to make 30 cycles of square wave-like motion between two visual markers attached to the setup, being paced by a metronome with the frequency 0.667 Hz.

The parameters F_p and F_n and the function $\Phi(v)$ were identified as explained in Section 2.3. Other parameters were chosen

as follows. The compliance K was set as $K = 1.2 \times 10^6$ N/m, which is close to the elasticity of the device that can be obtained through a close observation of the graph of Fig. 3. The constant α was chosen as $\alpha = 20.0$ s⁻¹ so that q_k converges to p_k reasonably quickly. The frequency of dither Ω_d was chosen as $\Omega_d = 15.0 \times 2\pi$ rad/s, which is larger than the frequency of typical human motion, assuming that external force is applied by a human user. The constant R_d was set to be 1.0.

The results from one typical cycle of the square-wave-like motion of the experimenter are shown in Fig. 6. In the cases **C** and **CD**, the force peaks appear at each velocity reversal, where the actuator produces the compensation force opposite to the experimenter's force. One can also see that the velocity peaks in the case **C** is larger than those in the cases **CD**, **P** and **PD**. The large velocity peaks in the case **C** are considered to be caused by the abrupt direction reversal of the compensation force.

The measured external force in each case was statistically analyzed by taking averages and standard deviations of the peak values in each motion direction and in each case. Each peak value was taken from a range with a constant interval 1.5 s as shown by the dashed lines in the bottom panel of Fig 6. Figure 7 shows the results. It can be seen that the average value is smallest in the case **PD**, and that the dither contributes the reduction of the force by comparing the cases **P** and **PD** and by comparing **C** and **CD**.

5.2 Experiment: Setup B

In the experiment using Setup B, the experimenter grasped the grip on the force sensor and intended to cyclically move it in a square-shaped trajectory in the x - y plane, being paced by a metronome with the frequency 0.667 Hz. The parameters were chosen as: $K = 50000$ Nm/rad, $F_p = F_n = 6.85, 9.56, 3.15$ Nm for each joint, $\alpha = 20$ s⁻¹, $\Omega_d = 30\pi$ rad/s and $R_d = 0.3$. They are chosen along similar guidelines to those explained in Section 5.1

Figures 8 and 9 show the results. As a whole, these figures show the same features as the results from Setup A; the average value is smallest in the case **PD** where the proposed compensator (18) with the dither was used.

From these results, we can conclude that the proposed method **PD** enhances the backdrivability of the device.

6. Further Improvement for 'Hand-Drivabilization'

6.1 Additional Algorithm for On-Line Adjustment of α

Considering applications in which the robot is 'hand-driven,' i.e., is moved by hand, a perfect friction compensation is not always beneficial because it causes unnecessary fluctuation of the robot motion especially when the user intends to stop the motion. In such an application, the friction should be appropriately compensated when the user intends to start moving, but the friction compensation should be weakened when the motion slows down.

As has been briefly explained in Section 4.1, the output force decays at the rate α when the velocity is smaller than $\alpha F/K$. For the static friction state, α should be a nominal value to realize an appropriate friction compensation, but in the kinetic friction state, the compensation force should decay quickly once the speed is sufficiently small. Based on this observation, here we propose an additional algorithm to adjust α in realtime, specifically for the 'hand-drivabilization.' This algorithm is a simple

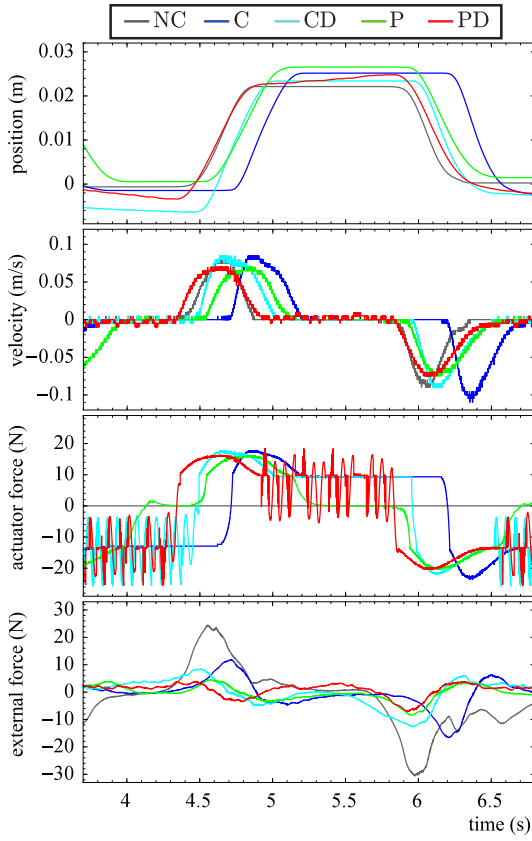
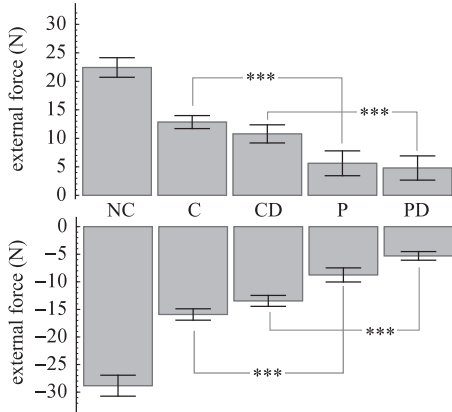


Fig. 6 One cycle of experimental results, Setup A.

Fig. 7 Averages and standard deviations of the peak values of the measured external force, Setup A. The triple asterisk (***) stands for the significant difference at $p < 0.1\%$ according to Student's t-test.

extension of the algorithm **algFC** as follows:

$$\text{Function } \mathbf{algFC2}(p_k) \quad (23a)$$

$$\text{If } |(p_k - p_{k-1})/T| > V_W \quad (23b)$$

$$w_k := \max(w_{k-1} + R_W, 1) \quad (23c)$$

$$\text{Else} \quad (23d)$$

$$w_k := \min(w_{k-1} - R_W, 0) \quad (23e)$$

$$\text{Endif} \quad (23f)$$

$$\alpha := (1 - w_k)\alpha_N + w_k\alpha_H \quad (23g)$$

$$\text{Return } \mathbf{algFC}(p_k, \alpha). \quad (23h)$$

Here, α_N is the nominal value of α , which has been used for the non-adaptive cases, and α_H is a value that is much higher than

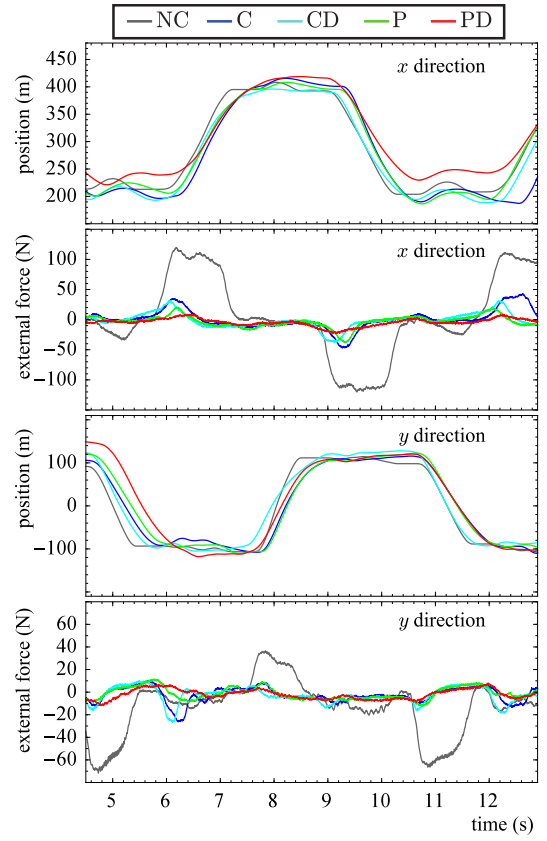
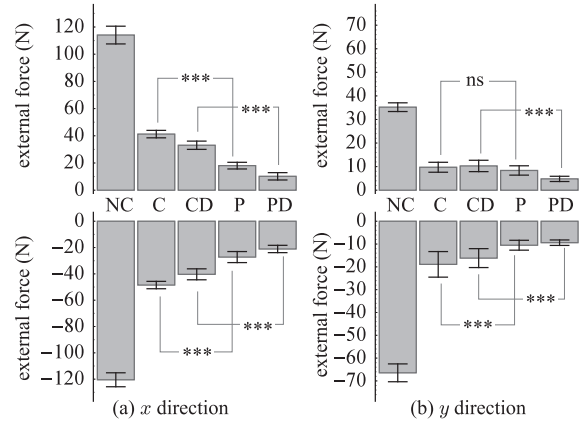


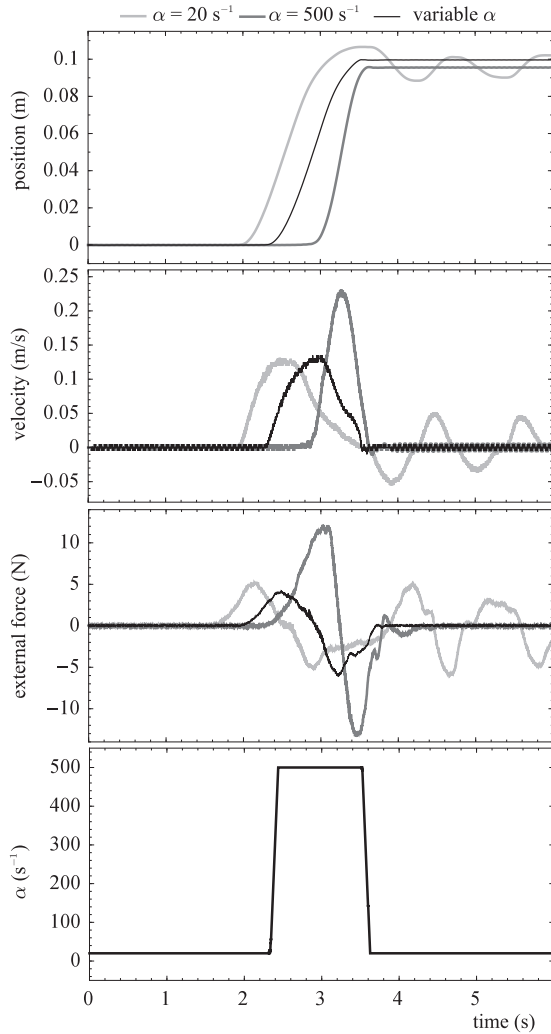
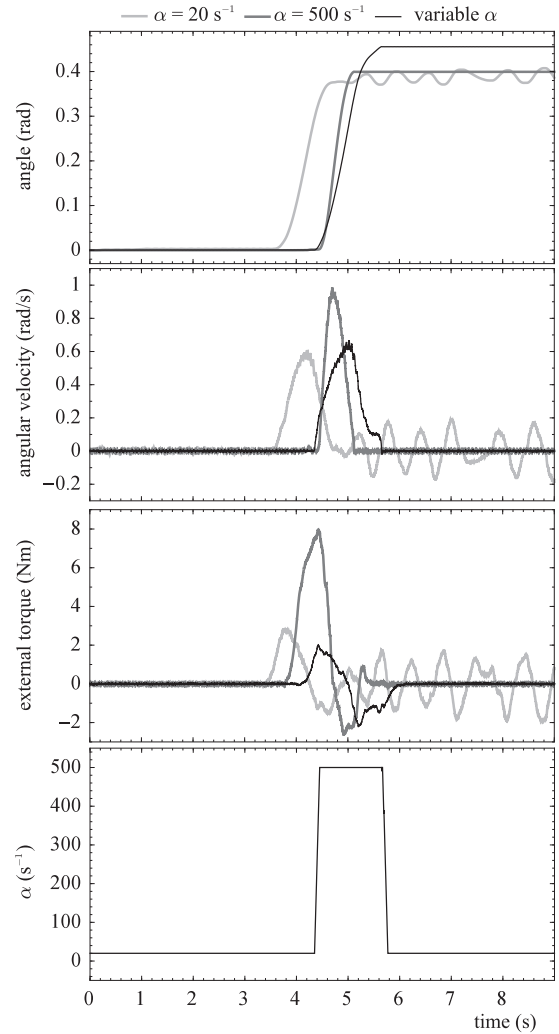
Fig. 8 One part of experimental results, Setup B.

Fig. 9 Averages and standard deviations of the peak values of the measured external force in each direction, Setup B. The triple asterisk (***) and 'ns' stand for the significant difference at $p < 0.1\%$ and no significant difference, respectively, according to Student's t-test.

α_N . The constant R_W determines the rate of change of α . The constant V_W is a threshold velocity below which α is decreased and above which increased.

6.2 Experiments

The algorithm **algFC2** in (23) was also tested with the two devices, Setup A and Setup B. In both setups, we set $\alpha_N = 20 \text{ s}^{-1}$ (which is the same value as in the experiments in Section 5), $\alpha_H = 500 \text{ s}^{-1}$ and $R_W = 0.01$. The value of α_N , the nominal value, was chosen for the same reason as for α in Section 5, the value of α_H was chosen to be sufficiently larger than α_N , and the value of R_W was chosen so that the transitions between $\alpha = \alpha_N$ and $\alpha = \alpha_H$ take place appropriately quickly.

Fig. 10 Results with variable α , Setup A.Fig. 11 Results with variable α , Setup B.

The velocity threshold was set at $V_W = 0.01$ m/s in Setup A and $V_W = 0.005$ rad/s in Setup B. The dither magnitude parameter was set as $R_d = 0.5$ in Setup A and $R_d = 0.2$ in Setup B, which are lower than those in Section 5 because, in an application of the ‘hand-drivabilization,’ a certain level of friction should be left uncompensated to suppress unnecessary fluctuation. The other parameters were set the same as in Section 5.

The following three cases were compared: $\alpha \equiv \alpha_N$, $\alpha \equiv \alpha_H$, and the case with the proposed algorithm **algFC2** in (23) with the varying α . With each of Setup A and Setup B, the experimenter grasped the grip of the end-effector of the setup, and moved it from a point to another point. With Setup B, only the joint 0 was used and the other joints were locked by local angle controllers.

The results with Setups A and B are shown in Figs. 10 and 11, respectively. These figures show mostly the same features. With the proposed algorithm **algFC2**, the force peaks were smaller than the other cases and the joint eventually came to stationary. This is in contrast to the case of the nominal α ($\alpha \equiv \alpha_N$), with which the fluctuation continued, and also to the case with the high α ($\alpha \equiv \alpha_H$), with which the force peaks were larger.

7. Conclusion

This paper has presented an elastoplastic friction compensator with some improvements. In the static friction state, the output force of the proposed compensator exponentially decreases to zero so that the compensator does not hamper the sensitivity to external forces. The proposed method also includes a dither-like friction compensation in the static friction state to enhance the backdrivability. Experiments using two different types of setups show that the proposed method effectively cancels the effects of joint friction in the devices, enhancing the sensitivity of the systems to the external forces. We have also presented an additional algorithm to reduce undesirable fluctuation of the joints when the device is driven by a human user’s hand.

Future work should clarify some guidelines for the choice of the parameters in the new compensator. Theoretical properties of the compensator, which is described as a differential algebraic inclusion in the continuous-time domain, is also an open problem.

Acknowledgments

This work was supported in part by Grant-in-Aid for Scientific Research (15H03938) from Japan Society for the Promotion of Science (JSPS).

References

- [1] M. Iwatani and R. Kikuuwe: An elastoplastic friction compensator with improved static friction behavior, *Proceedings of SICE Annual Conference*, pp. 1091–1097, 2016.
- [2] V. Hayward and B. Armstrong: A new computational model of friction applied to haptic rendering, P. Corke and J. Trevelyan, Eds., *Experimental Robotics VI*, ser. Lecture Notes in Control and Information Sciences, Vol. 250, pp. 404–412, Springer-Verlag, 2000.
- [3] P. Dupont, V. Hayward, B. Armstrong, and F. Altpeter: Single state elastoplastic friction models, *IEEE Transactions on Automatic Control*, Vol. 47, No. 5, pp. 787–792, 2002.
- [4] R. Kikuuwe, N. Takesue, A. Sano, H. Mochiyama, and H. Fujimoto: Admittance and impedance representations of friction based on implicit Euler integration, *IEEE Transactions on Robotics*, Vol. 22, No. 6, pp. 1176–1188, 2006.
- [5] X. Xiong, R. Kikuuwe, and M. Yamamoto: A multistate friction model described by continuous differential equations, *Tribology Letters*, Vol. 51, No. 3, pp. 513–523, 2013.
- [6] M. Mahvash and A.M. Okamura: Friction compensation for enhancing transparency of a teleoperator with compliant transmission, *IEEE Transactions on Robotics*, Vol. 23, No. 6, pp. 1240–1246, 2007.
- [7] M. Iwatani, R. Kikuuwe, and M. Yamamoto: Friction compensation of harmonic drive gearing based on parallel viscoelastoplastic friction model, *Journal of Robotics Society of Japan*, Vol. 32, No. 5, pp.445–455, 2014 (in Japanese).
- [8] T. Tjahjowidodo, F. Al-Bender, H. Van Brussel, and W. Symens: Friction characterization and compensation in electro-mechanical systems, *Journal of Sound and Vibration*, Vol. 308, No. 3, pp. 632–646, 2007.
- [9] F. Al-Bender, V. Lampaert, and J. Swevers: The generalized Maxwell-slip model: A novel model for friction simulation and compensation, *IEEE Transactions on Automatic Control*, Vol. 50, No. 11, pp. 1883–1887, 2005.
- [10] M. Iwatani and R. Kikuuwe: An identification procedure for rate-dependent friction laws of robotic manipulator with limited motion range, *Proceedings of the 10th Asian Control Conference (ASCC)*, pp. 526–530, 2015.
- [11] R. Kikuuwe, N. Takesue, and H. Fujimoto: A control framework to generate nonenergy-storing virtual fixtures: Use of simulated plasticity, *IEEE Transactions on Robotics*, Vol. 24, No. 4, pp. 781–793, 2008.
- [12] M.T.S. Aung, R. Kikuuwe, and M. Yamamoto: Friction compensation of geared actuators with high presliding stiffness, *Transactions of ASME: Journal of Dynamic Systems, Measurement, and Control*, Vol. 137, No. 1, 011007, 2015.

Ryo KIKUWE (Member)



He received his B.S., M.S. and Ph.D. (Eng.) degrees from Kyoto University, Kyoto, Japan, in 1998, 2000, and 2003, respectively, all in Mechanical Engineering. From 2003 to 2007, he was an Endowed-Chair Research Associate at Nagoya Institute of Technology, Nagoya, Japan. Since 2007, he has been an Associate Professor at the Department of Mechanical Engineering, Kyushu University, Fukuoka, Japan. From 2014 to 2015, he was a Visiting Researcher at INRIA Grenoble Rhône-Alpes, France. His research interests include physical human-robot interaction, real-time simulation for physics-based animation, and engineering applications of differential inclusions.

Masayoshi IWATANI



He received his B.S. and M.S. degrees in Mechanical Engineering from Kyushu University, Fukuoka, Japan, in 2012 and 2014, respectively. Since 2014, he has been pursuing a Ph.D. degree in Mechanical Engineering from Kyushu University. His research interests include friction compensation, physical human-robot interaction, and control of bipedal robot.